STATE RESEARCH CENTER OF RUSSIA

INSTITUTE FOR HIGH ENERGY PHYSICS

NuMI–B–543

September 30, 1999

Advanced Conceptual Design of the Low Energy Target and Beam Plug

(Task E Report of the Accord between FNAL and IHEP)

A.Abramov, V.Ferapontov, P.Galkin, N.Galyaev, V.Garkusha,
V.Gres, A.Kharlamov, E.Lomakin, F.Novoskoltsev,
A.Ryabov, V.Zapolsky, V.Zarucheisky

Protvino 1999

Contents

1 Target for the Low Energy Neutrino Beam **3**

1.1 Outline 3

1.2 Target Design 4

1.3 Target Cooling 6

1.4 Energy Deposition, Temperature and Stress Calculations . . 6

1.5 Mounting of the Target in the Beam Line 8

1.6 Conclusions 9

2 Beam Plug for the Low Energy Neutrino Beam **26**

2.1 Outline 26

2.2 Plug Design 27

2.3 Energy Deposition, Temperature and Stress Distributions . . 28

2.4 Conclusions 29

1 Target for the Low Energy Neutrino Beam

1.1 Outline

The low energy (LE) configuration of the PH2 focusing system [1, 2] provides a wide band neutrino beam for the MINOS experiment in the energy range of 1–6 GeV. To maximize a number of neutrino events in the far detector, the LE target is placed inside the first horn on 2/3 of its length; therefore the maximum transversal size of a target design is limited by the internal diameter of the horn inner conductor at the downstream end of the target and should be less than 40 mm. Moreover, the thickness of main elements of a target design, i.e. target casing and a cooling system, should be thin enough to minimize the absorption of secondaries which are produced by a primary proton beam in the target core.

Descriptions of four initial conceptual designs of the LE target, which differ by cooling of the target (forced water or gas convection) and the shape of a target core (cylindrical or fin), are given in the 1999 Task C IHEP Report [3]. Graphite ZXF-5Q of Poco Graphite, Inc. and beryllium S-65C of Brush Wellman, Inc. have been considered as possible target core materials for each of the LE target design. As neutrino beam simulations show, the difference in production efficiencies (ν_μ charged current event rates in the far detector) between all presented target designs does not exceed 5%.

Taking into account that,

- even under the static pressure of 1.0–1.2 MPa in the cooling system, gas cooled targets have the average temperature significantly higher than that for water cooled targets,

- for both medium and high energy configurations of the PH2 focusing system targets assumed to be water cooled [1],

water cooling is looked as more preferable for the LE target. Two problems of the construction of water cooled LE targets (encapsulating of a cylindrical graphite target core into a stainless steel pipe and brazing of a fin graphite target core to cooling pipes) were verified at the stage of their initial conceptual design by means of manufacturing of ~30 cm long samples, which correspond to the downstream part of the target.

As for the shape of a target core, the detailed analysis of LE target designs given in the previous IHEP Report shows that:

- in the case of water cooling the fin target allows to avoid an interaction between the mis-steered primary proton beam and elements of a cooling system and target casing. The maximum allowable excursion of a primary proton beam in the focusing system is determined by baffle protection collimators [1], which prevent direct hitting of horn necks by the mis-steered proton beam. Figure 1.1 shows possible trajectories of a primary proton beam with respect to main elements of the LE focusing system for given radii of baffle collimators;

- the fin target is operationally more flexible than the target with cylindrical core, e.g. for higher intensity of a primary proton beam one could spread the beam further in the vertical direction keeping the energy deposition density and, correspondingly, a temperature rise and stresses at the same level as for the baseline intensity;

- the sag of a target due to its own weight is noticeable less for a fin target, moreover it may be not taken into account because the beam spot size in this direction is significantly larger than the sag.

Giving somewhat preference to graphite as a target core material meaning its ease and safety machining, the water cooled graphite fin target has been considered as a baseline design for the LE beam configuration.

1.2 Target Design

Results given in [3] show, that at the primary proton beam spot size with $\sigma_x = 0.7$ mm and $\sigma_y = 1.4$ mm and focusing of a beam in the target in the horizontal plane with dispersion equal to zero, the length of a target segment (tooth) equal to 20 mm corresponds to the maximum equivalent stress of 22.5 MPa, what is acceptable for the long term target operation. In this case two interaction lengths target should consist of 47 segments.

Taking into account possible locations of a proton beam provided by the baffle protection system (Figure 1.1), the distance between the beam line axis and cooling pipes should be equal at least to 10 mm. Two possible configurations of the target cross-section with the external diameter of cooling pipes equal to 4 mm are given in Figure 1.2. Variant "A" has slightly lower

luminosity (in a few percents) but is more rigid and at the same velocity of a cooling water its temperature rise is two times lower with respect to variant "B". Variant "A" is taken here for further consideration, although the final choice of a cross-section will be done after more detail study of a brazing technology by manufacturing and testing of samples for both variants.

The target design is shown schematically in Figures 1.3–1.6. Figure 1.3 shows general view, Figures 1.4 and 1.6 — upstream and downstream parts of the target respectively and Figure 1.5 — some details of the design.

The target core consists of 47 target segments brazed in a vacuum by an electron beam to four stainless steel pipes with the external diameter of 4 mm and the wall thickness of 0.2 mm (view B-B, Figure 1.5). Copper-titanium is used as a brazing filling material.

The target segment is machined out by an electrical discharge machine from ZXF-5Q graphite sheet and has following sizes: 3.2 mm thickness, 28 mm height and 20 mm length. In order to decrease the stress concentration at segment corners, they are rounded with a radius of rounding equal to the half of thickness (view F-F, Figure 1.5). The place of brazing of the graphite sheet is coated preliminary in a vacuum by thin (3-5 microns) copper layer and heat-treated in a vacuum during 5–10 minutes at the temperature about 950°C.

The target core with brazed cooling pipes is inserted into stainless steel target casing (32 mm in diameter with a wall thickness of 0.3 mm) and is fixed by means of three aluminum spacers. Aluminum spacers are anodized with alumina (30 μm in thick) to provide an insulation of the target core for "Budal" monitor.

The metal-ceramic (high alumina) adapters between target casing and the ground, as well as in water cooling piping are applied in order to prevent the electrical discharge from the first horn to the target (see Figure 1.3). The insulation of target casing to the ground will also allow to measure the charge of casing similar to the "Budal" signal.

The fixture (see Figure 1.4 and view D-D, Figure 1.5) prevents any forces to the target core which arise during the target assembly. A special anodized aluminum casing support is used in order to relieve the metal-ceramic adapter welded to target casing.

There are two collectors in the cooling system as it is shown in a view E-E, Figure 1.5. Two bellows prevent any forces to the metal-ceramic

adapters which arise in the design during assembly and operation. Inlet and outlet water pipes, as well as the pipe for vacuum pumping (or gas filling) are made of flexible metal pipes in order to provide necessary degree of freedom during target mounting.

The target canister with a ConFlat flange will provide the tightness of a target core volume. Two beryllium windows separate the internal volume from surrounding environment.

1.3 Target Cooling

The energy deposition in target segments was calculated by MARS [4]. The results of calculations for the base line intensity of $4{\cdot}10^{13}$ protons/spill are given in Figure 1.7. The total deposited energy is equal to 5.08 kJ and for the repetition period of 1.9 s it corresponds to the power of 2.67 kW. The power deposited in a cooling system due to particle interactions with a water and stainless steel cooling pipes is equal to 0.37 kW. So, the total load to the cooling system is equal to 3.04 kW.

Calculations show, that at the total water flow rate of 3.4 l/min (water velocity 3 m/s) a water temperature rise is equal to 12°C and at the roughness of cooling pipe of 0.02 mm the pressure drop is equal to 1.0 atm.

The energy deposited in the 0.3 mm thick stainless steel target casing is equal to 640 W. It corresponds to the power flux through the lateral surface (surface of heat exchanging with surrounding atmosphere) of about 6.8 kW/m^2. Measuring of a casing temperature heated by d.c. current shows that at this power and a natural convection the casing temperature reaches the value of ~300°C. It corresponds to the heat transfer coefficient equal to 20–25 W/m^2/K. The use of 0.5 mm thick aluminum casing allows to reduce the deposited power to the value of 209 W and even at a natural convection the casing temperature will be about 95°C. The upstream end of the target in the case of aluminum casing is shown in Figure 1.8. The transition from aluminum to stainless steel can be made using technology applied for similar transitions in the cooling system of target prototypes [5].

1.4 Energy Deposition, Temperature and Stress Calculations

The two–dimensional distribution of the energy deposition density corresponding to its maximum along the target length (6-th segment) is shown

in Figure 1.9. The maximum density of an energy deposition is equal to 0.092 GeV/cm^3/proton. Temperature distributions and quasi-static thermal stresses in a fin target segment were computed by the finite element program HAST [6] at the following conditions:

- heat transfer coefficient to the water is equal to 10 kW/m^2/K;
- water cooling temperature rise is taken into account: the water temperature at its input is equal to 20°C, the water temperature at its output is equal to 32°C;
- thermal resistance between the target segment and cooling pipes is equal to zero;
- ambient temperature is equal to 20°C;
- radiation is taking into account for the coefficient of blackness equal to one;
- heat transfer coefficient to the ambient atmosphere is equal to zero, i.e. target is in the vacuum.

Temperature distributions in the target along the vertical axis ($x = 0$) just before and after the beam spill at a steady state is shown in Figure 1.10. The maximum temperature after the beam spill is equal to 344°C and the adiabatic temperature rise $\Delta T = 288$°C. The steady state is reached in 4–5 proton spills.

Two–dimensional distributions of stresses in the middle cross-section of a target segment in the case when the beam center-weight coincides with the target center are shown in Figure 1.11 ($z = 0$) and in Figure 1.12 ($y = 0$). The maximum equivalent stress equal to 22.5 MPa takes place in the center of the target segment ($x = y = z = 0$) and corresponds to the all-axis compression ($S_{xx} = -3.6$ MPa, $S_{yy} = -16.3$ MPa and $S_{zz} = -29.6$ MPa). It is very important because the maximum ultimate strength of the ZXF-5Q graphite is compressive strength of 170 MPa.

As it follows from Figure 1.12, there is a stress concentration at segment corners ($x = \pm d/2$, $z = \pm L/2$, where d is the target segment thickness and L is the segment length). In order to avoid the stress concentration, these corners should be rounded. The dependence of the equivalent stress as a

function of the radius of corner rounding was computed by ANSYS and results of calculations are given in Figure 1.13. Rounding of target corners with the radius equal to 1.6 mm (one half of the segment thickness) decrease the stress from 41 MPa to 25.6 MPa.

In case of a mis-steered primary proton beam in the horizontal plane, the maximum of an equivalent stress shifts from the segment center to lateral surfaces. Stresses in the most crucial points $(\pm d/2;0;0)$ of the target segment as functions of a beam position are shown in Figures 1.14. Stresses for mis-steered beam are higher than those when the beam is centered well, but they are considerable lower (31.3 MPa) than the ultimate tensile strength of graphite (90 MPa). Taking into account that the beam is deflected from the center of the target only during very short period of a time, the target will not be destroyed. When the long term stability of a beam location in the target equal to ± 0.3 mm is provided, stresses on lateral surfaces of the target segment do not exceed the value of 25.6 MPa.

1.5 Mounting of the Target in the Beam Line

There are two ways to mount the target inside the upstream part of the first horn. The first one is that the target has its own filler module and another one — to mount the target to the outer conductor of the first horn. The common feature of both ways is that the target should be insulated to the ground and to the horn in order to prevent discharge between the horn inner conductor and the target due to very high ionization in a target area. Both ways should also provide the 0.8 mm accuracy of a target position with respect to the first horn in the transverse direction. It is necessary for predicting the far detector energy spectrum from measurements in the near detector to $\leq 2\%$ in the worst 1 GeV energy bin.

The way of target mounting to the filler module is shown in Figure 1.15. There is the special flange for clamping of the target to the filler module. All water, vacuum (or gas) piping, as well as electrical cabling, pass through the hole in a filler module to the top of a shielding.

The design in the case of target mounting to the horn is shown schematically in Figure 1.16. Four bolts of the inner and outer conductor junction are used to connect the conical flanged branch to the inner conductor flange. This conical branch has some holes for pipes (cooling system, vacuum or gas) and electrical cables. An insulation of the horn to the target is pro-

vided by eight high alumina ceramic plugs. The thickness of an insulation is equal to 5 mm.

Let us compare these two ways of target mounting:

- The target is mounted on its own filler module
  - because of the beam axis sloped to the horizon, the proper location of the target can be provided by simultaneous movement of a filler module along the beam axis and lowering of the target by the driving system of a filler module. A special driving system is necessary to move a filler module in the horizontal plane along the beam;
  - in case of the target (or horn) failure there is no need to replace the horn (or target);
  - in case of need to dismantle the target there is no need to design remote controlled or fast-disconnected connectors (electrical, water, vacuum or gas).

- The target is mounted on the first horn
  - the horn flange and adjoined target parts should be made with high precision to provide needed accuracy of a target position;
  - in case of the target (or horn) failure the whole assembly (target and horn) should be replaced;
  - in case of need to dismantle the target it is necessary to design remote controlled or fast-disconnected connectors (electrical, water, vacuum or gas) to minimize the personal radiation exposure.

1.6 Conclusions

Given above the advanced conceptual design of the water cooled target for the low energy neutrino beam confirms the reality of its creation. The main features of this target design are:

- the target consists of 47 graphite segments brazed in a vacuum with an electron beam to four stainless steel cooling pipes; the geometrical sizes of the target design are thus chosen that direct hitting of the cooling system by a primary proton beam is excluded;

- taking into account the long term stability of a proton beam position in the horizontal plane (± 0.3 mm), stresses in a target do not exceed 25.6 MPa; this value is lower than an estimated value (36 MPa) of the fatigue limit of the ZXF-5Q graphite;
- increasing of stresses to 31.3 MPa due to a mis-steered proton beam in the horizontal plane are not so serious taking into account a short duration of its action;
- the insulation of the target to the ground and to the first horn is made of high alumina ceramic at the upstream end of the target; the insulation allows to avoid the possible discharge from the target to horn and to receive "Budal" signal for proton beam position monitoring;
- the target may be mounted to the first horn or to the separate filler module.

Finally, the production efficiency of the LE target design described in this Report (variant "A" of a cross-section) has been compared with that of the 0.94 m long and 3.2 mm radius graphite rod target. This rod target gives the largest number of ν_μ CC events with $E_\nu \leq 6$ GeV in the far MINOS detector among considered earlier different targets for the LE beam configuration of the PH2 focusing system (see Figure 1.3 of the last IHEP Report [3]). Results of calculations, which were made using the GNuMI beam simulation software, are shown in Figure 1.17. Besides of decreasing of an average density of the target core (due to rounding of target segments), main details of the LE target design, i.e. water cooling pipes and target casing, were taken into account.

As it follows from these results, for the "real" LE target design the number of ν_μ CC events in the far detector is 10% less in the energy range of $E_\nu \leq 6$ GeV than for the 3.2 mm radius rod target. Mentioned above variant "B" of the LE target design gives $\sim$2% greater the neutrino event rate than the described in details variant "A".

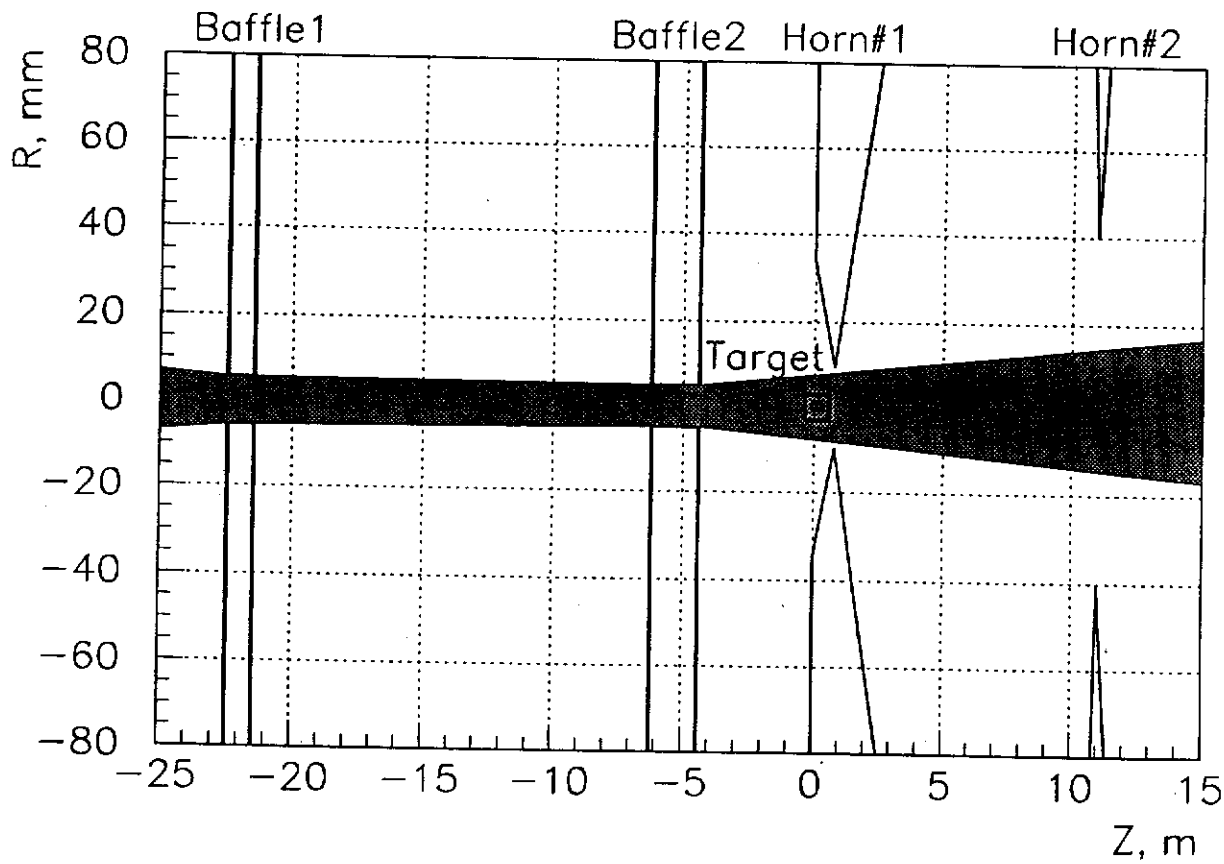

Figure 1.1: Schematic drawing of the LE focusing system with baffle protection collimators. Shaded area means possible trajectories of a primary proton beam.

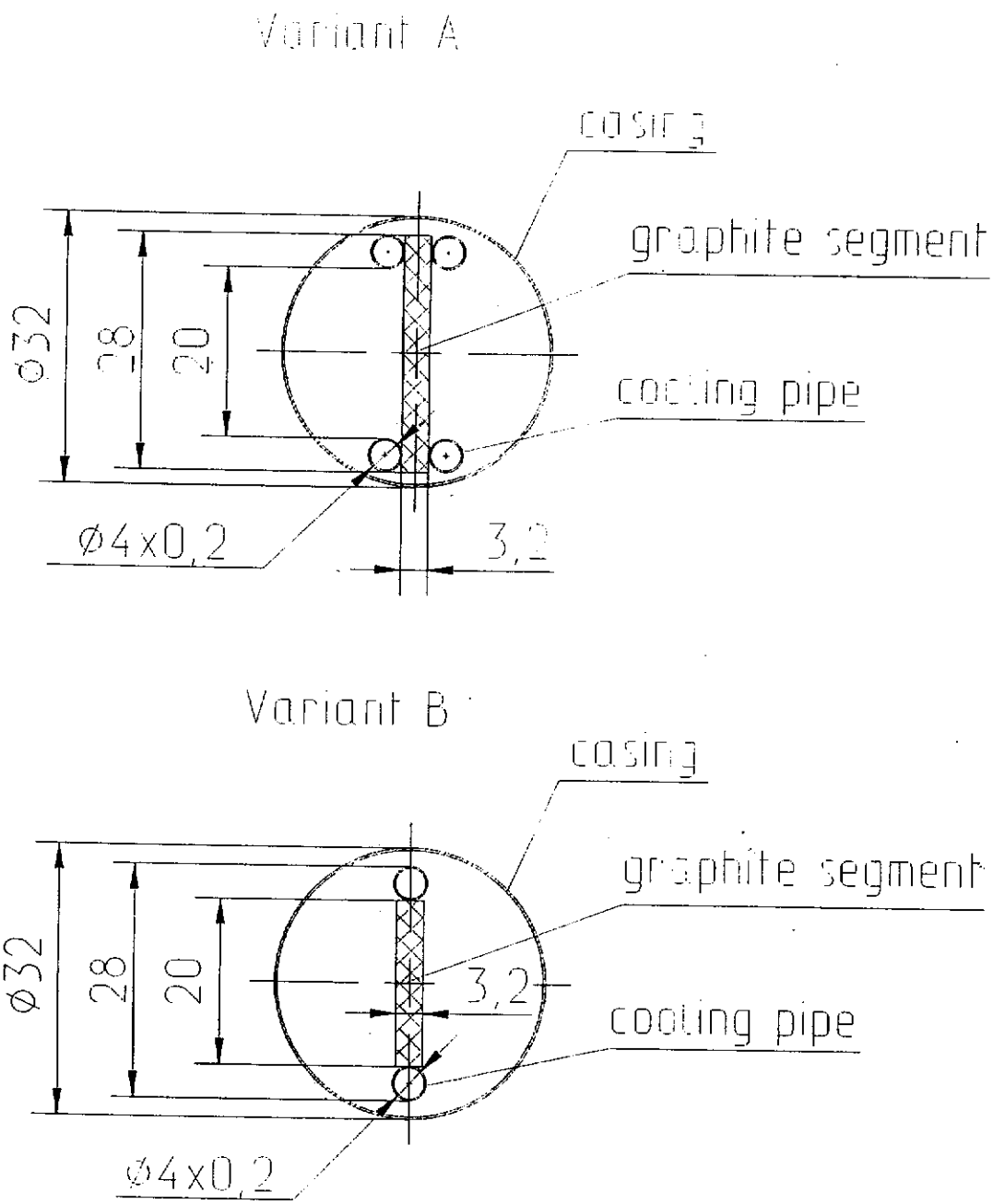

Figure 1.2: Possible configurations of the LE target cross-section. "+" indicates the water input, "–" indicates the water output.

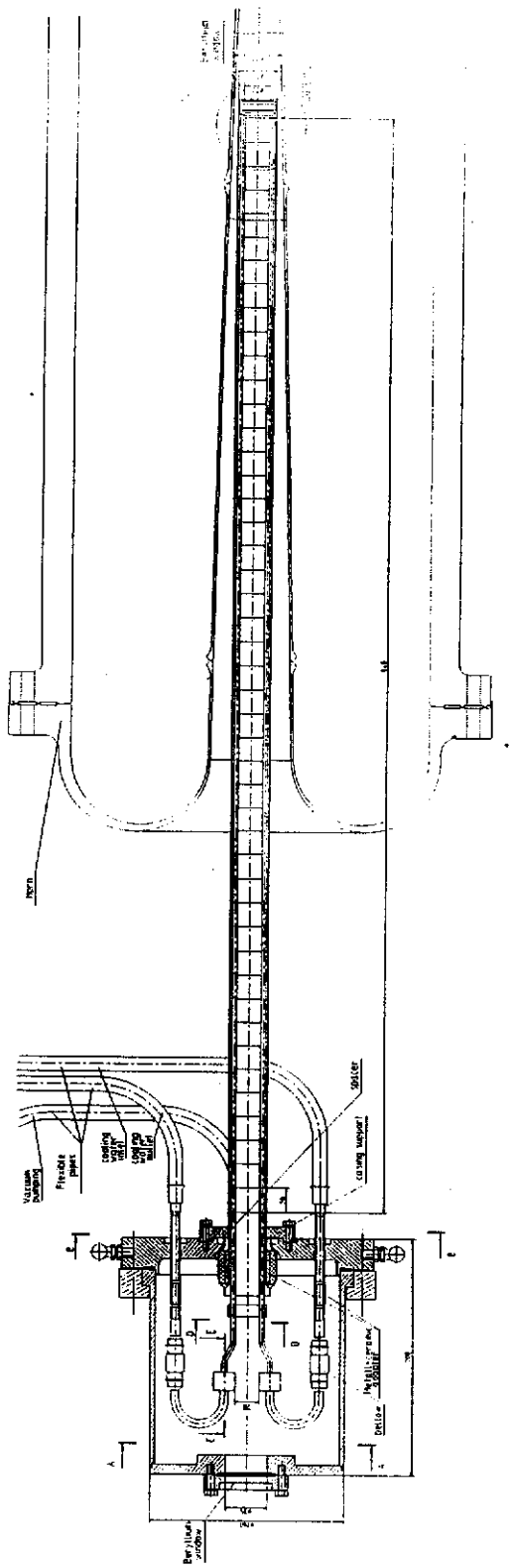

Figure 1.3: The general view of the LE target design.

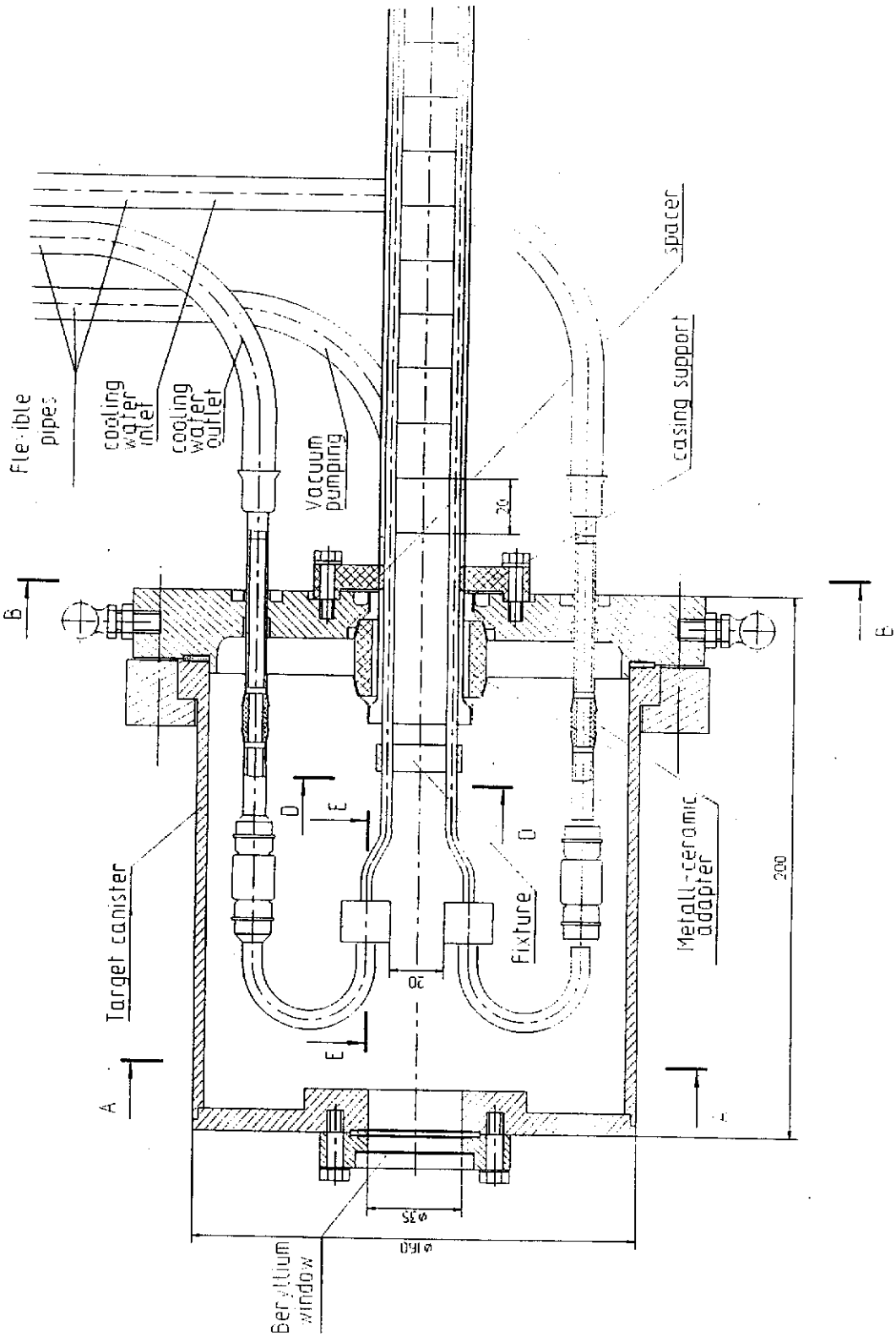

Figure 1.4: The upstream end of the target.

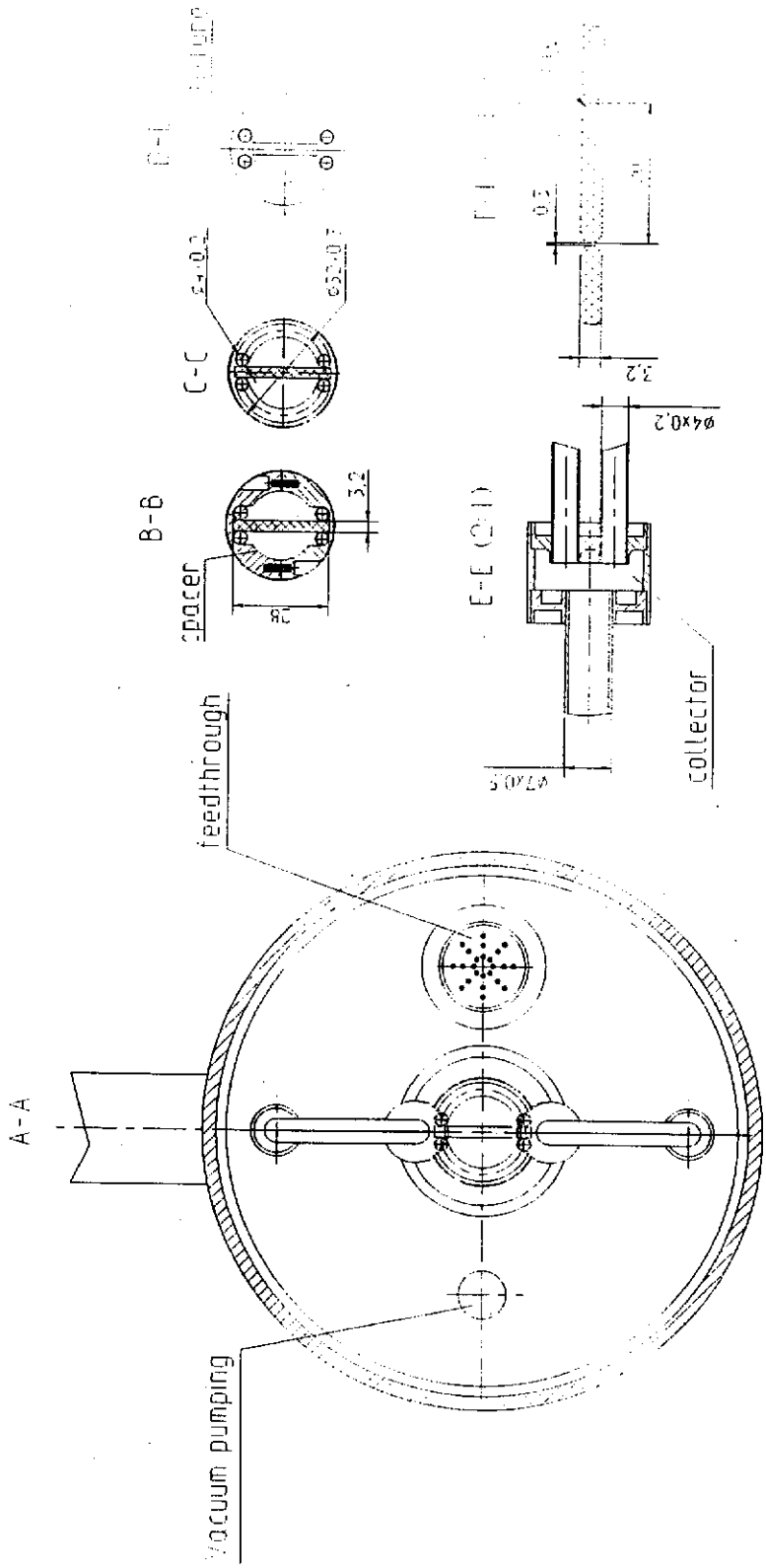

Figure 1.5: Some details of the target design.

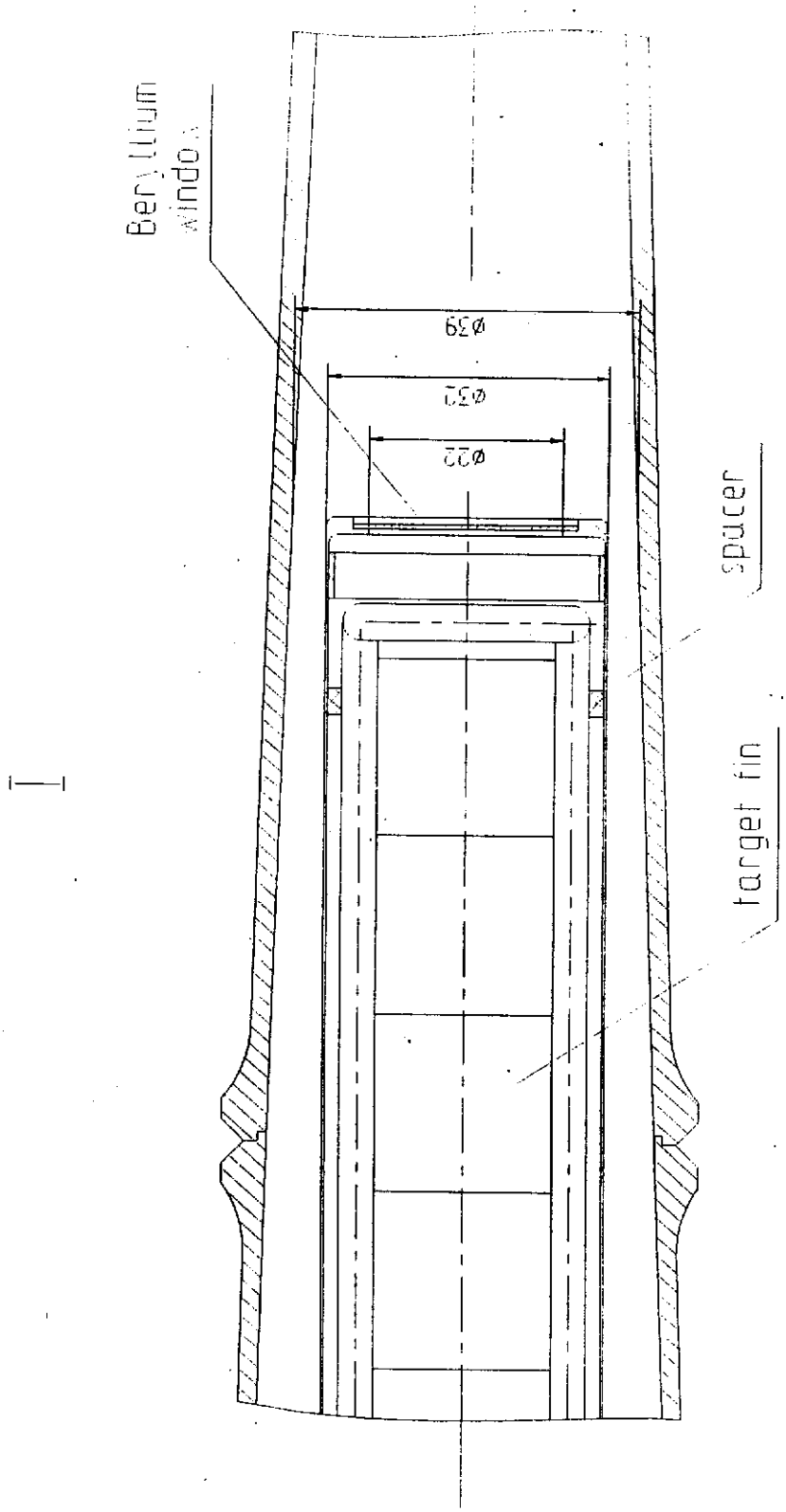

Figure 1.6: The downstream end of the target.

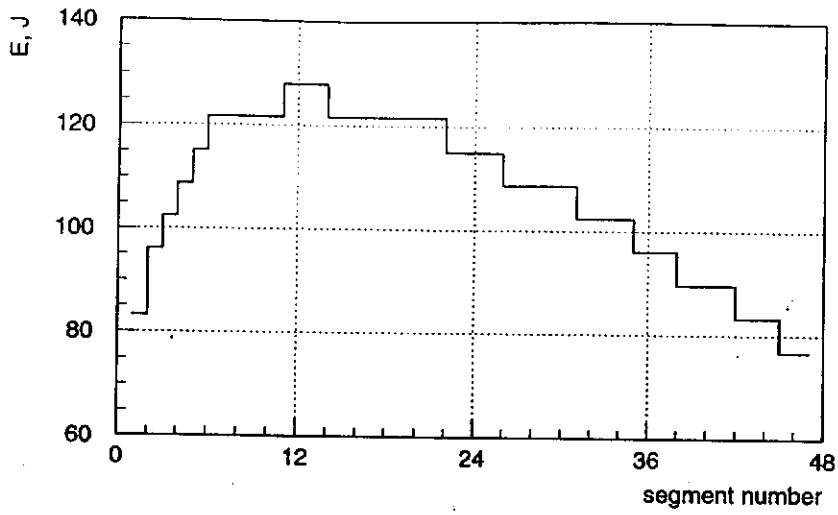

Figure 1.7: The energy deposition distribution in target segments.

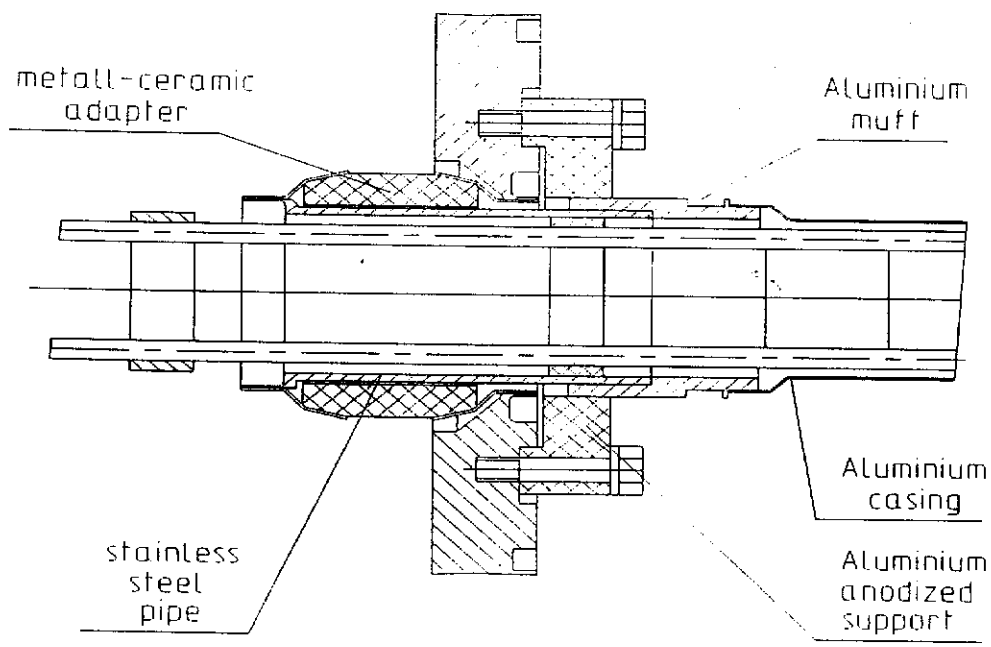

Figure 1.8: The upstream end of the target with aluminum casing.

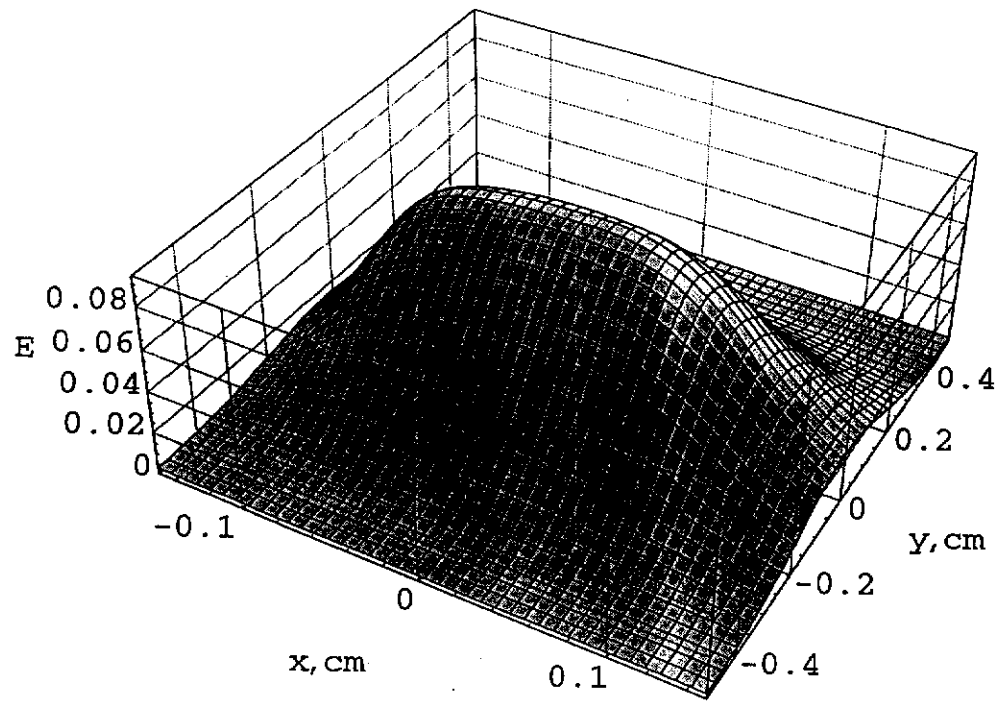

Figure 1.9: The transversal distribution of the energy deposition density (GeV/cm^3/proton) in the target segment.

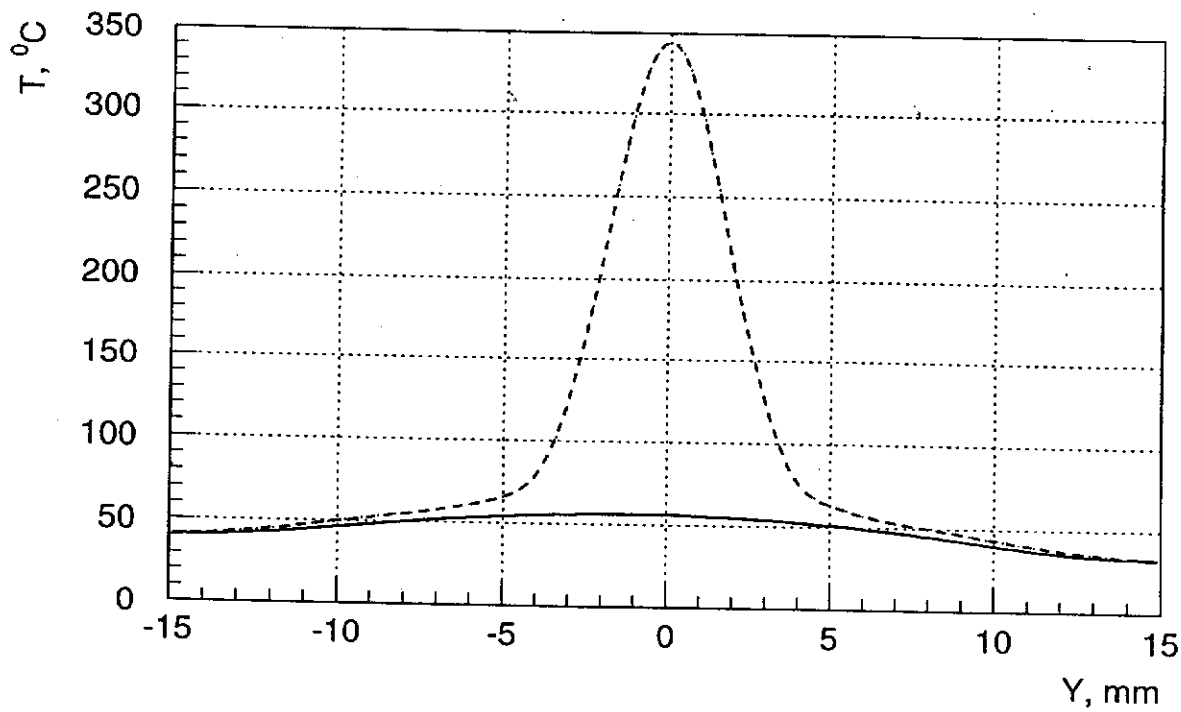

Figure 1.10: Temperature distributions in the target segment along the vertical axis before (solid line) and after (dashed line) spill.

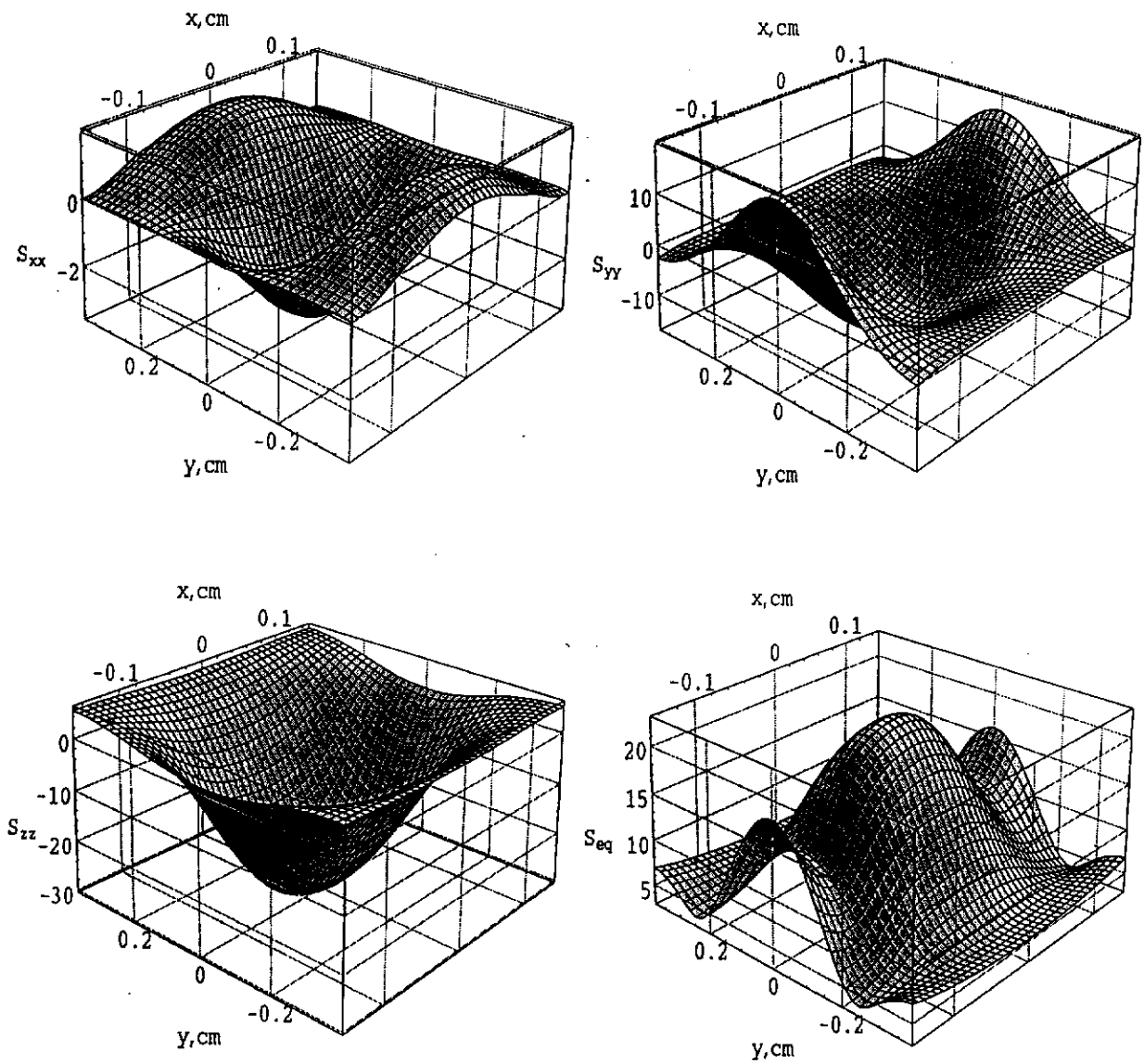

Figure 1.11: Stresses (MPa) in the middle cross-section ($z = 0$) of the target segment.

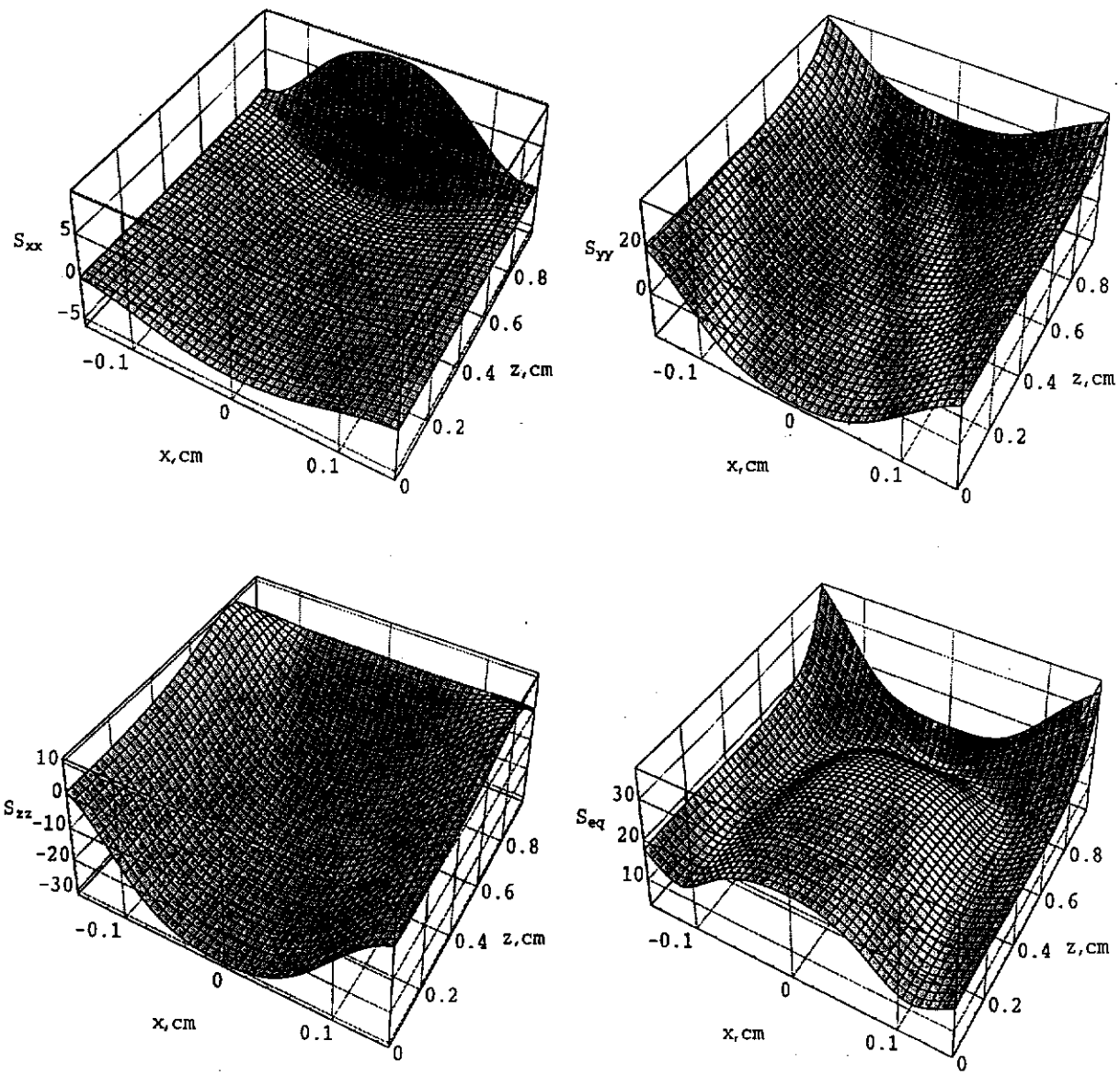

Figure 1.12: Stresses (MPa) in the middle cross-section ($y = 0$) of the target segment.

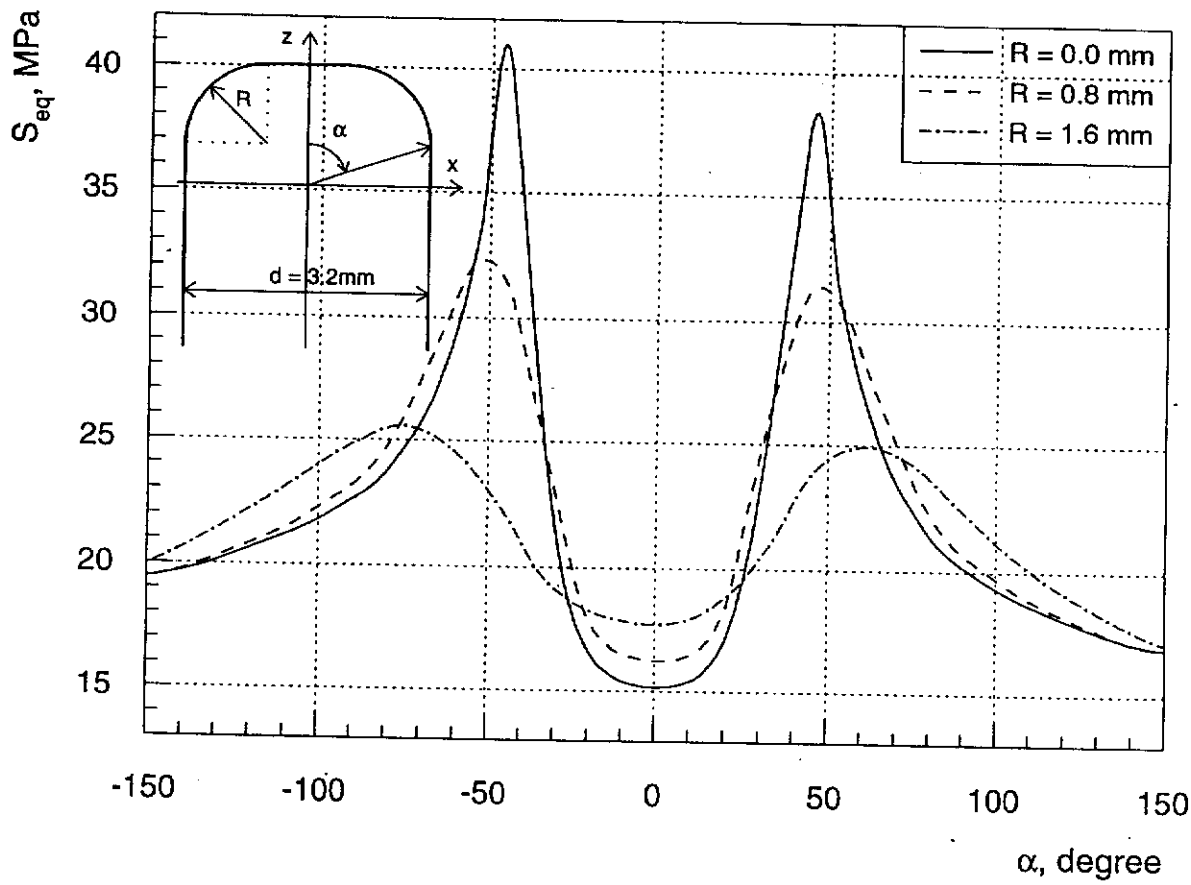

Figure 1.13: The stress concentration in corners of the target segment.

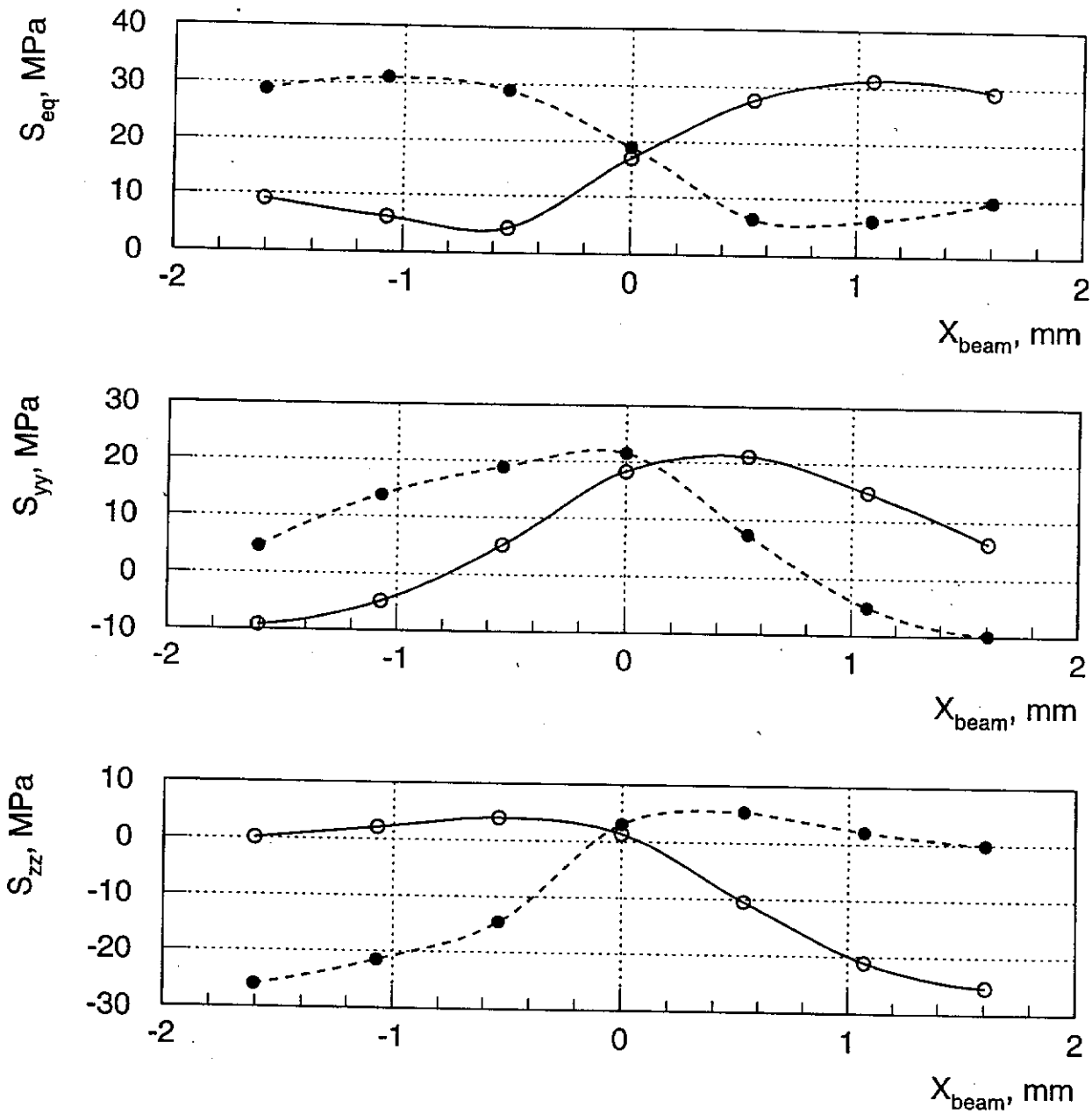

Figure 1.14: Stresses in the target segment as functions of the beam center position in the horizontal direction. Solid lines correspond to the point $(+d/2;0;0)$, dashed lines correspond to the point $(-d/2;0;0)$, where d is the thickness of the target segment.

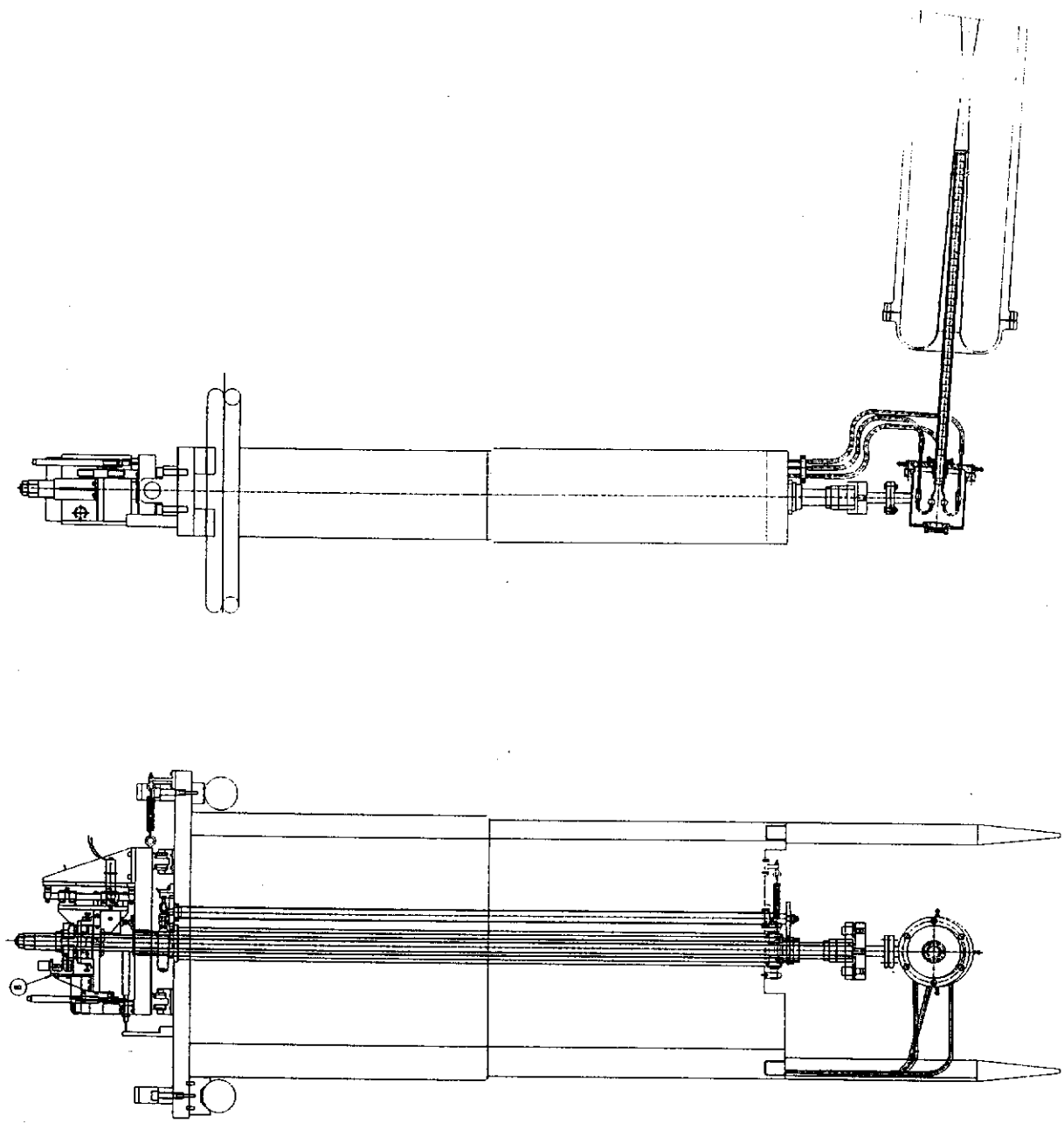

Figure 1.15: The general view of the LE target mounted on the separate filler module.

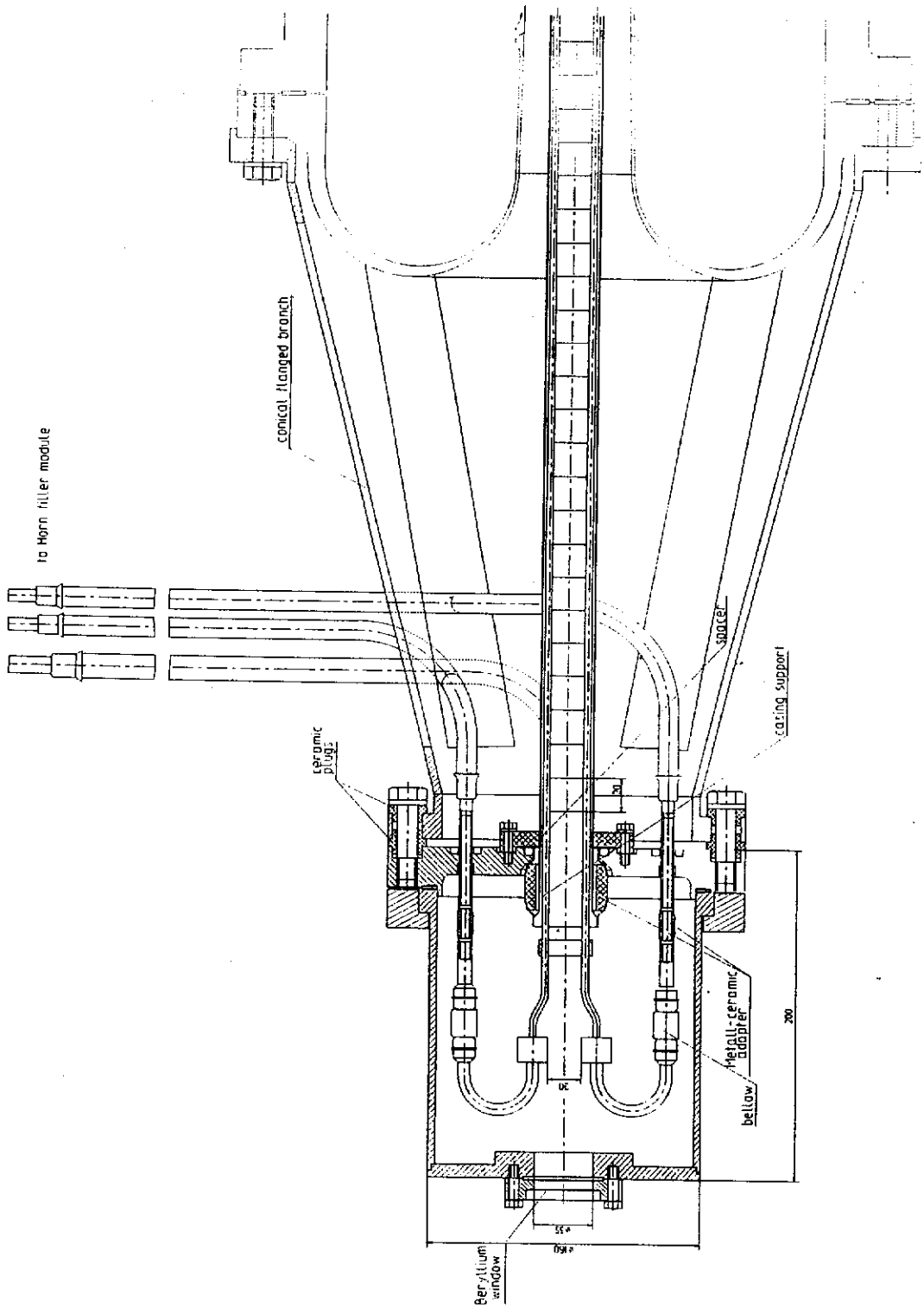

Figure 1.16: The general view of the LE target mounted on the first horn.

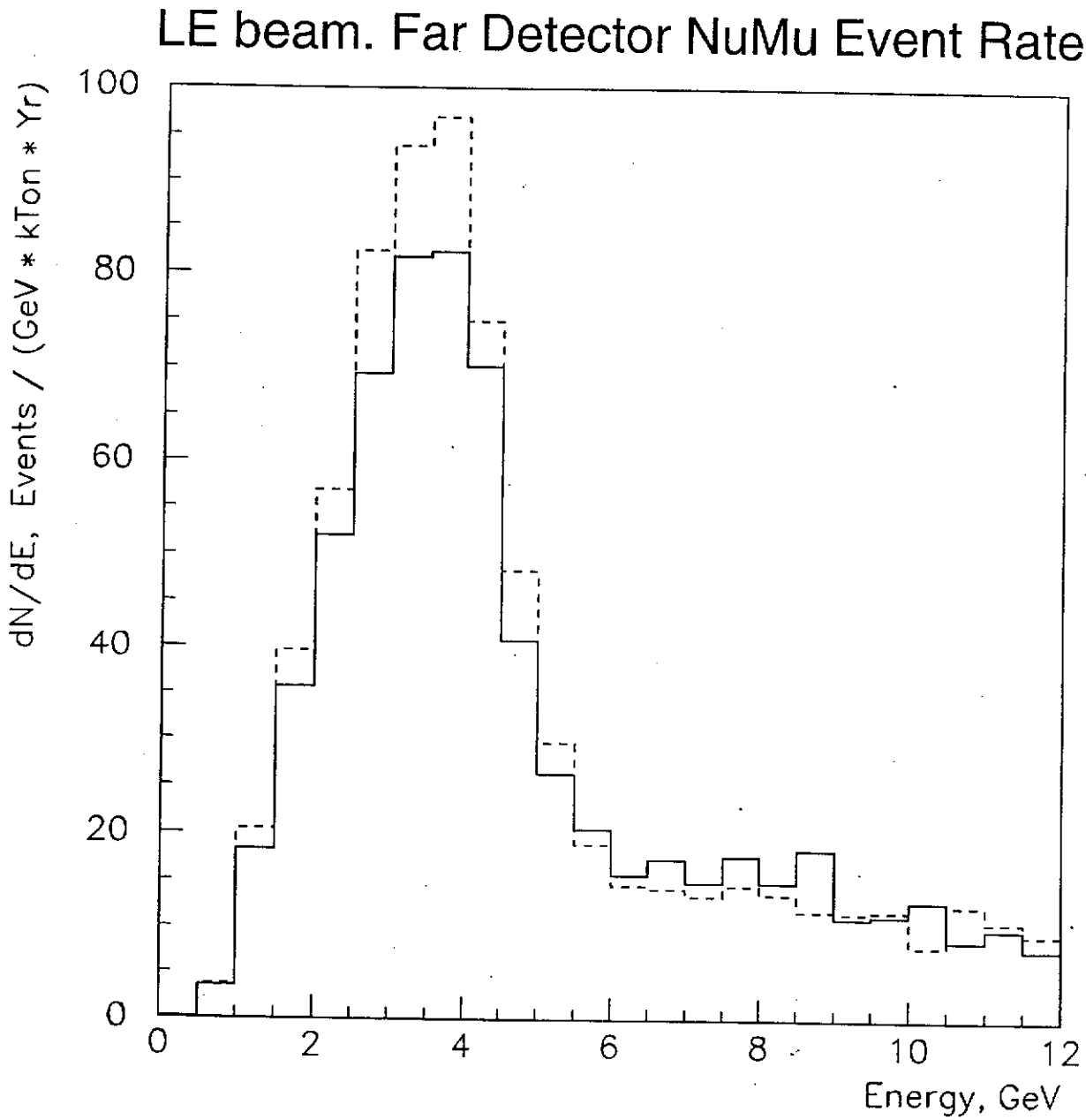

Figure 1.17: Energy spectra of ν_μ CC events in the far detector for the LE beam configuration with the water cooled fin target described in this Report (solid line) and with the 3.2 mm radius rod target (dashed line).

2 Beam Plug for the Low Energy Neutrino Beam

2.1 Outline

In the LE neutrino beam spectrum shown in Figure 1.17 there are a lot of neutrino events in the energy region $E_\nu \geq 6$ GeV which can produce a background in some oscillation tests. The high energy tail of the neutrino spectrum may be suppressed with help of a beam plug placed in the focusing system to absorb the most of high energy parents contributing in this part of the neutrino spectrum, but without large losses of low energy parents. Therefore, there should be a strong correlation between momenta and transverse positions of parent particles for the optimal position of the beam plug. On the other hand, its position should provide a simple installation and removing of the plug.

So far as in an emergency situation the beam plug should withstand a full intensity primary proton beam passing the target, graphite was considered as a possible material for the plug core. The radius of a graphite core in the beam plug should be large enough to avoid an interaction between a primary proton beam and a plug cooling system, which is made of more dense materials than the plug core. Possible trajectories of a primary proton beam with respect to main elements of the LE focusing system are shown in Figure 1.1.

The effects of the graphite plug placed closely to the downstream end of the first horn depending on its length and radius on the LE neutrino spectrum are illustrated in Figure 2.1. Beam simulations have been made by the M.C. program HALO, which takes into account absorption and scattering of neutrino parents in a plug material, but without generation of secondary particles. No details of the beam plug design (cooling system, casing etc.) have been included in these calculations.

As it follows from presented plots, the variation of a plug length changes the absorption efficiency of very forward parents and, correspondingly, the suppression efficiency of highest energy neutrino events. On the other hand, the variation of a plug radius changes the energy below what the neutrino beam has not great losses of the event rate in the far detector. Somewhat loss of $E_\nu = 1$–2 GeV neutrino events is caused by the partial absorption of low energy pions overfocusing by the first horn on the beam plug.

2.2 Plug Design

The general view of the plug design is shown in Figure 2.2. Taking into account given above results and inventory sizes of Poco Graphite, Inc. for cylinders, the plug core was accepted 1.5 m (5×300 mm) in length and 31.7 mm in diameter. ZXF-5Q graphite rods are encapsulated in a stainless steel pipe with help of zone-normalized deformation method:

- core rods are placed inside a metal pipe with a small gap equal to 0.05–0.1 mm;
- stainless steel pipe is stretched in the longitudinal direction and heated locally to the temperature exceeded the elastic limit with help of an electron beam gun moving along the pipe axis;
- to provide uniform azimuthal heating, the pipe is rotated around its axis.

At the initial stage of cooling the metal pipe shrinks plastically. When the temperature drops below inelastic limit, the pipe shrinks elastically. The value of a prestress can be estimated by the following expression:

$$P_0 \simeq (\alpha_m - \alpha_t) E_m \Delta T \, a / r_0,$$

where α_t is the thermal expansion coefficient of a plug material, α_m is the thermal expansion coefficient of a metal pipe, E_m is the elasticity modulus of a metal pipe, ΔT is the temperature inelastic limit, a is the thickness of a metal pipe and r_0 is the plug core radius.

For the graphite core and 16X12M2C2 stainless steel (Russian grade widely used in nuclear reactors) $E_m \simeq 200$ GPa, $\Delta T \simeq 600°$C, $\alpha_m - \alpha_t = 3 \cdot 10^{-6}$ K^{-1} and at the thickness of an external pipe $a = 0.2$ mm, the prestress $P_0 \simeq 4$ MPa. This prestress is sufficient in order to provide good thermal contact between the graphite core and stainless steel pipe.

Two beryllium windows seal and separate the plug core in a dry helium (or nitrogen) environment. Helium (or nitrogen) is supplied through the 1 mm diameter pipe. To fill all volume of a plug core by gas, core rods are machined out as it is shown in Figure 2.2.

Cooling water passes from the downstream end to the upstream one inside water channel formed by internal and external pipes. The gap between

these pipes is equal to 2 mm. Cooling water inlet and outlet are made of stainless steel pipe 10 mm diameter and with the 0.5 mm wall thickness. The thickness of the external stainless steel pipe is chosen 0.3 mm. As a result, the thickness of the plug in the transverse direction coincide to the ~18.5 mm graphite rod.

The plug is bolted to the support of the filler module by two rods with muffs connected to the plug in Euler points to minimize the sag. Two adjustment bolts are used to provide the proper angular position of the plug with respect to the beam line direction.

The upstream part of low energy beam configuration in case when the target is mounted to the filler module is shown in Figure 2.3.

2.3 Energy Deposition, Temperature and Stress Distributions

The reliability of a plug design is determined by temperature and stresses at the most crucial situation, when the 120 GeV primary proton beam with full intensity ($4{\cdot}10^{13}$ protons/spill) hits the plug core. The distribution of deposited energy was calculated by MARS for the proton beam spot size with $\sigma_x = 0.7$ mm and $\sigma_y = 1.4$ mm (the same as in the target).

In this case the distribution of deposited energy E along the plug is given in Figure 2.4a. The maximum energy deposition is equal to 3.14 kJ and corresponds to $z = 1$ m. Beyond this point, each additional 10 cm adds ~3 kJ to the total deposited energy and consequently ~1.5 kW to the total deposited power (Figure 2.4b). For the total length of plug equal to 1.5 m the deposited power is equal to 19.7 kW. The power deposited in a water cooling system (stainless steel pipes and a water) is about 4.9 kW, i.e. the total load to the cooling system reaches the value of 24.6 kW. Calculations show, that at flow rate 16.6 l/min (pressure drop $\Delta P = 1$ atm) the water temperature rise is equal approximately to 22.5°C.

In case when the proton beam is steered properly in the target (operational situation), the total deposited power in the plug is only 2.5 kW and consequently the water temperature rise is about 2.5°C.

Maximum stresses in the plug core will arise in the cross-section with maximal energy deposition density. The maximum density of an energy deposition is the same as in the graphite target and is equal to 0.092 GeV/cm^3/p. Temperature and stress calculations were made under following conditions:

- input water temperature is equal to 20°C;
- heat transfer coefficient to the water is equal to 10 kW/m^2/K;
- heat resistance between graphite and stainless steel (0.2 mm thick) casing is equal to zero;

The steady state temperature is reached in 10–12 proton spills. Temperature and equivalent stress distributions just after the beam spill in the cross-section corresponding to the maximum energy deposition density are shown in Figure 2.5 (top). For comparison, bottom part of this Figure gives similar distributions in the most heated cross-section ($z = 1$ m).

As it follows from these plots, in the cross-section where the density of deposited energy reaches its maximum, an equivalent stress is about 24 MPa and corresponds to the all-axis compression. In the most heated cross-section the adiabatic temperature rise, its gradient in the transverse direction and, consequently, stresses are significantly lower.

2.4 Conclusions

In conclusion one should note, that the main problem of a plug design is providing of a good thermal contact between the plug core and a cooling water. Solving of this problem proposes the use of zone-normalized deformation method for encapsulating of graphite rods ~32 mm in diameter into the stainless steel pipe. It was verified by manufacturing of the 300 mm length sample corresponding to the middle part of the plug. Sample testing confirms this possibility.

As for the LE target design presented in previous Section, an efficiency of the plug design is illustrated by results of neutrino beam simulations given in Figure 2.6 and Table 2.1. These results, which were obtained with help of the GNuMI taking into account main details of plug and target designs, show that the beam plug factor 2.4 decreases high energy part of the neutrino spectrum ($E_\nu > 6$ GeV) keeping its low energy part without noticeable changes. The ratio of ν_μ CC events at $E_\nu > 6$ GeV to those at $E_\nu < 6$ GeV decreases from 94% up to 40%.

Besides suppressing of a high energy tail in the LE beam spectrum the beam plug decreases the $\tilde{\nu_\mu}$ component of the background in the ν_μ beam. Beam simulations show, that the beam plug half as much decreases the

LE beam focusing system	ν_μ CC events per kTon*Year			
	$E_\nu < 3$ GeV	$E_\nu < 6$ GeV	$E_\nu > 6$ GeV	Total
without beam plug	89	250	234	484
with beam plug	83	244	98	342

Table 2.1: The LE beam neutrino event rate in the far detector.

number of $\tilde{\nu}_\mu$ CC events in the far detector intercepting the flux of negative pions passing without defocusing to the decay region through field free holes in the horn necks. At the same time, the fraction of $(\nu_e + \tilde{\nu}_e)$ events, giving the most dangerous background for oscillation experiments, remains almost without changes.

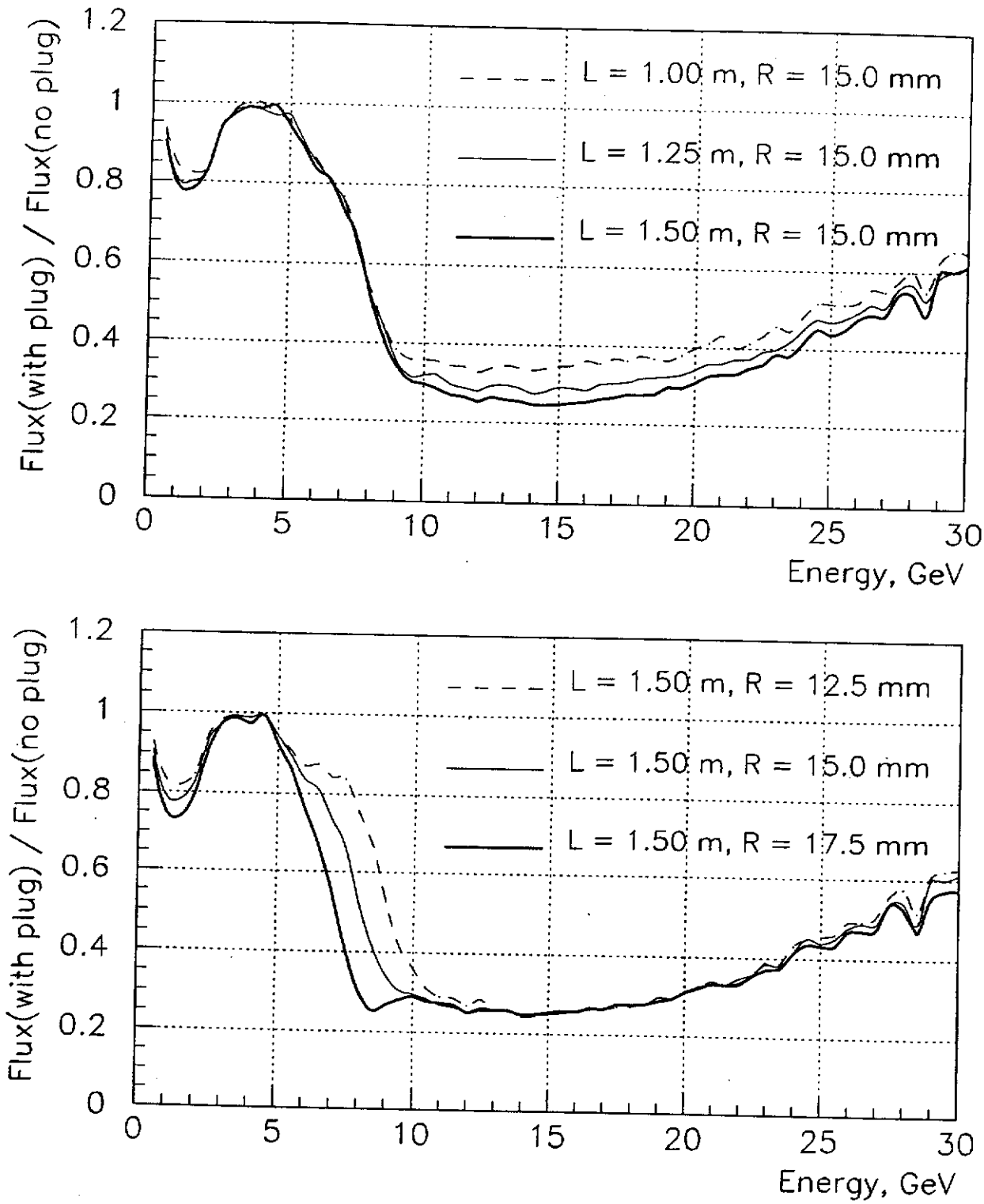

Figure 2.1: Ratios of neutrino energy spectra for the LE focusing system with the plug to that without the plug for various plug lengths and radii.

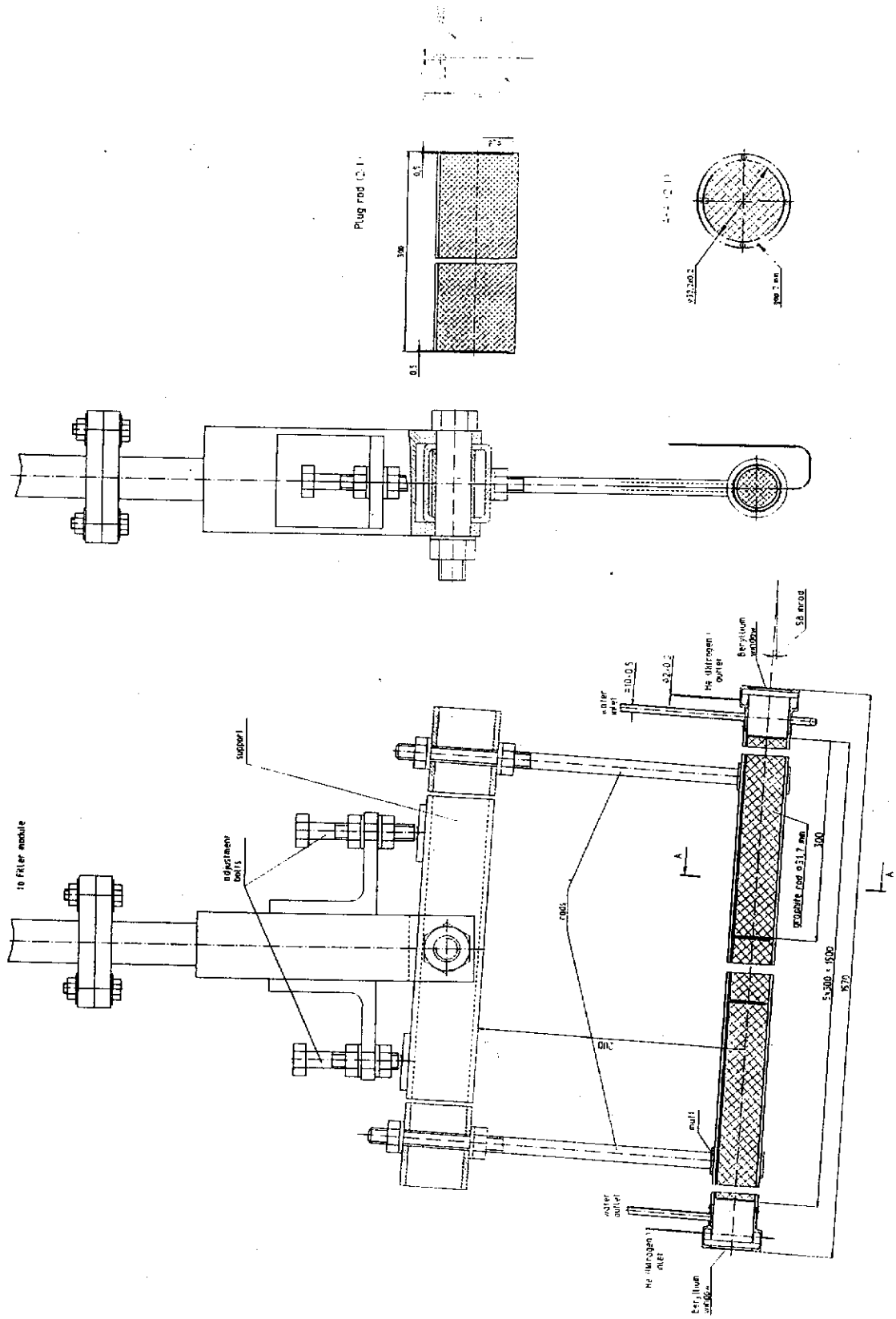

Figure 2.2: The general view of the beam plug design.

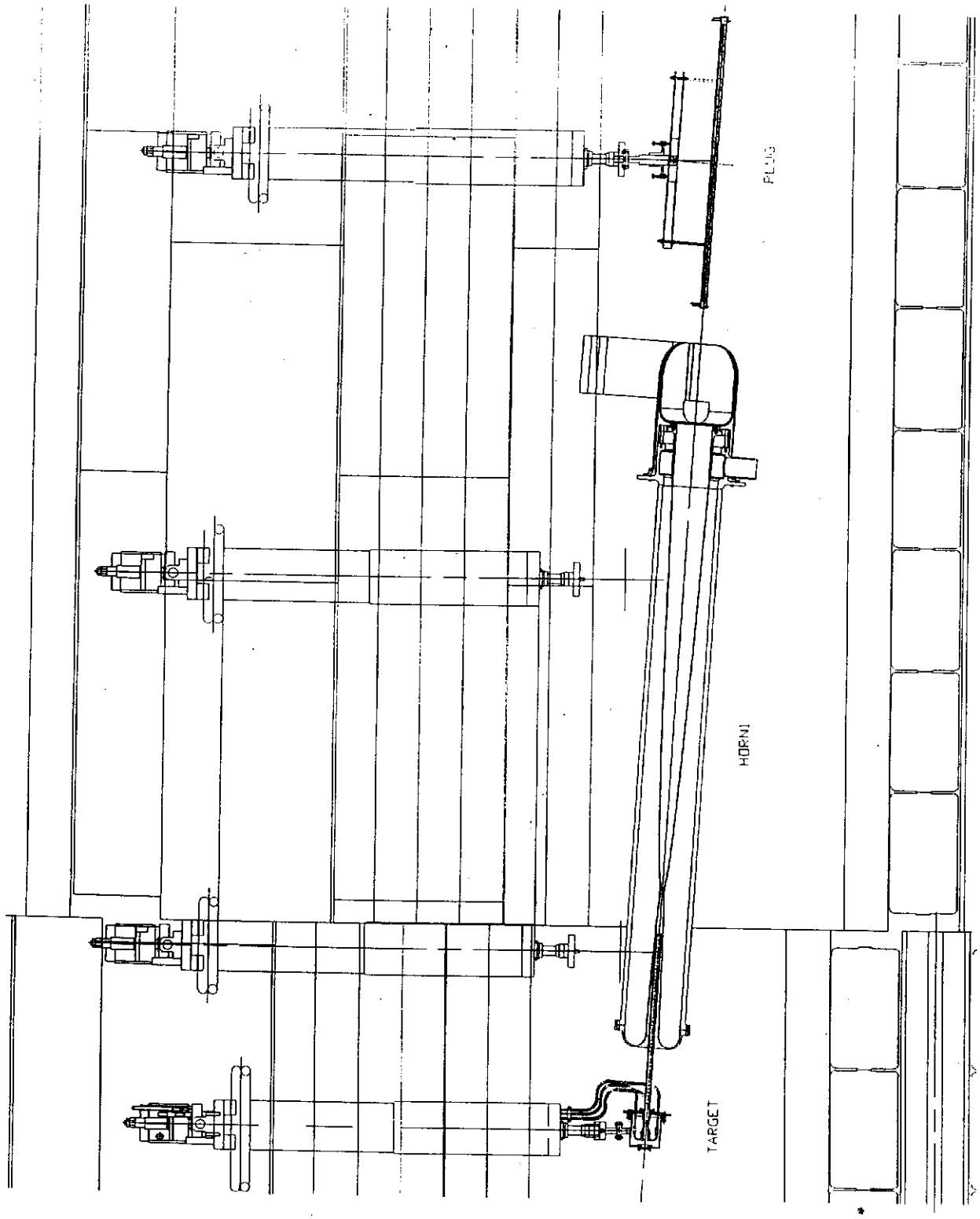

Figure 2.3: The upstream end of the LE beam configuration.

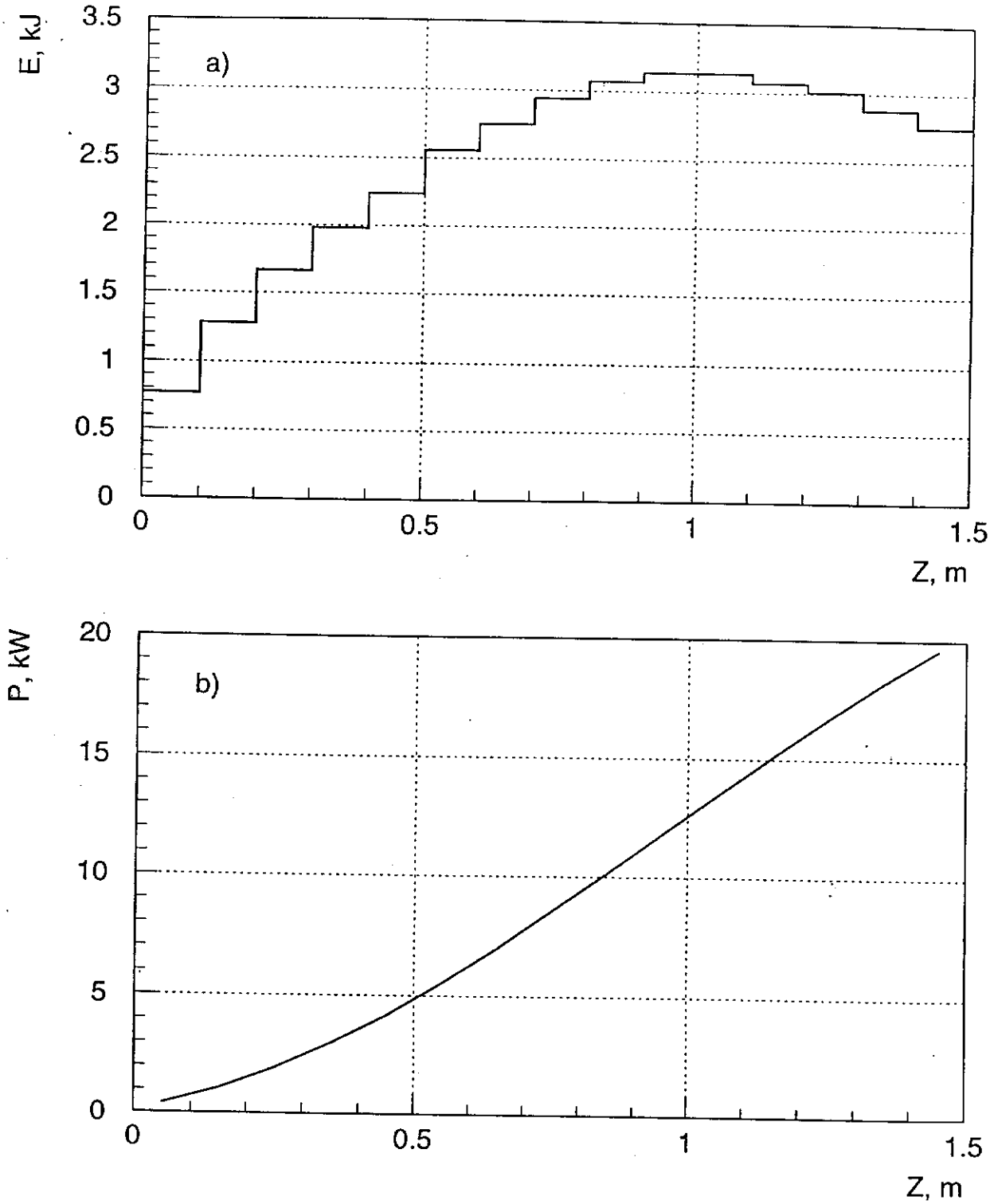

Figure 2.4: The energy deposition distribution along the beam plug (a) and the total average deposited power as a function of a plug length (b).

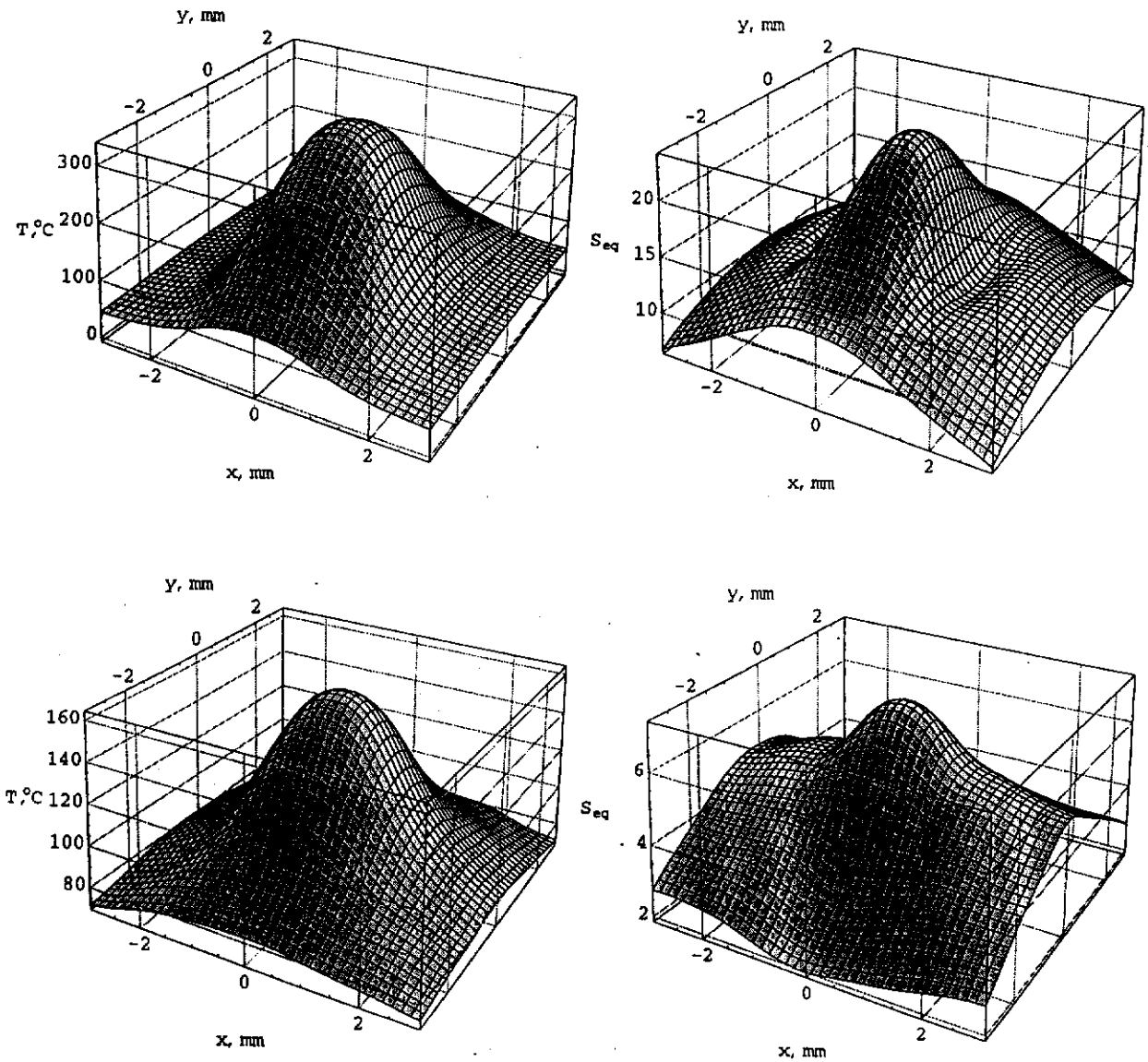

Figure 2.5: Temperatures (°C) and equivalent stresses (MPa) in two cross-sections along the plug. Top plots correspond to the maximum energy deposition density cross-section, bottom plots — to the most heated cross-section ($z = 1$ m).

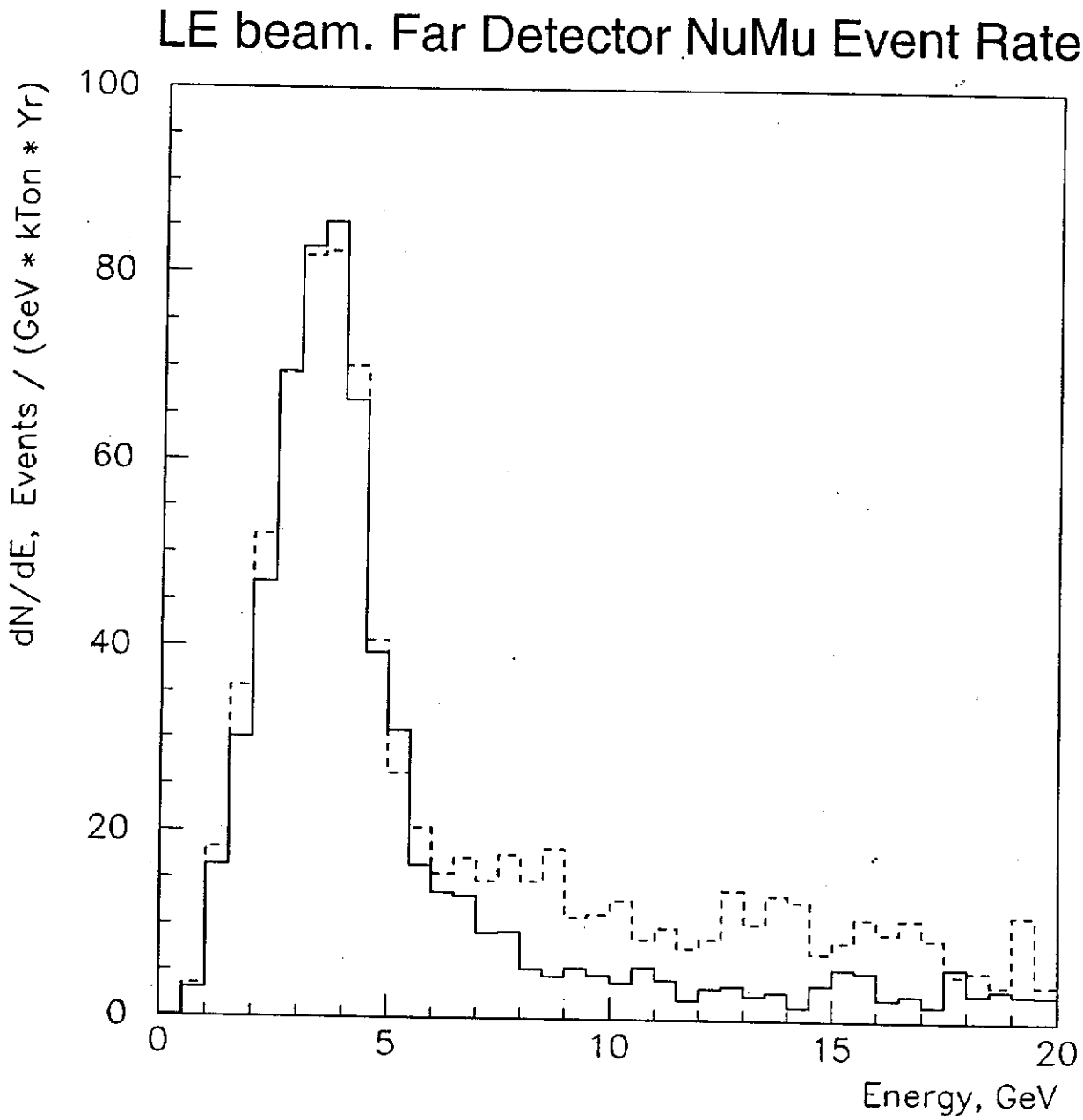

Figure 2.6: Energy spectra of ν_μ CC events in the far detector for the LE beam configuration with the addition of the beam plug (solid line) and without it (dashed line).

References

[1] The NuMI Facility Technical Design Report, Fermilab, 1998.

[2] The PH2M Two Horns Focusing System for the NuMI Project, Protvino, 1999, NuMI-B-471.

[3] Comparison of Initial Conceptual Designs of the Low Energy Target, Protvino, 1999, NuMI-B-501.

[4] Degtyarev I.I. et al., IHEP Preprint 94-119, Protvino, 1994.

[5] Advanced Conceptual Design of the Full Scale Fin Target and Engineering Design of the Target Prototypes for the NuMI Project, Protvino, 1998, NuMI-B-454.

[6] A.Abramov et al., IHEP Preprint 84-64, Serpukhov, 1984.